1999

Room Temperature Oxidation of Al-Cu-Fe and Al-Cu-Fe-Cr Quasicrystals

Patrick J. Pinhero
Iowa State University

Daniel J. Sordelet
Iowa State University

James W. Anderegg
Iowa State University, anderegg@ameslab.gov

Pierre Brunet
Centre d' Ingdnierie des Matériaux

Jean-Marie Dubois
Centre d' Ingdnierie des Matériaux

See next page for additional authors

Room Temperature Oxidation of Al-Cu-Fe and Al-Cu-Fe-Cr Quasicrystals

Abstract

We have investigated formation of oxides on quasicrystalline and crystalline alloy surfaces of similar composition, in different oxidizing environments. This includes a comparison between a quaternary orthorhombic approximate of Al-Cu-Fe-Cr quasicrystal and the ternary Al-Cu-Fe quasicrystalline and crystalline phases. We noted that each sample showed the following common trends: preferential oxidation of the Al, enrichment in the concentration of Al present at the surface upon oxidation, water concentration is directly related to oxide thickness, and the oxide thickness displays a strong correlation with the bulk concentration of Al in the sample.

Comments

This article is from *Quasicrystals: Proceedings of the MRS 1998 Fall Meeting* 553 (1999): pp. 263—268, doi:10.1557/PROC-553-263

Authors

Patrick J. Pinhero, Daniel J. Sordelet, James W. Anderegg, Pierre Brunet, Jean-Marie Dubois, and Patricia A. Thiel

ROOM TEMPERATURE OXIDATION OF Al-Cu-Fe and Al-Cu-Fe-Cr QUASICRYSTALS

PATRICK J. PINHERO [1,2], DANIEL J. SORDELET [3], JAMES W. ANDEREGG [1], PIERRE BRUNET [4], JEAN-MARIE DUBOIS [4], PATRICIA A. THIEL [1,2]
[1] Materials Chemistry Program, Ames Laboratory, Ames, IA 50011, [2] Dept. of Chemistry, Iowa State University, Ames, IA 50011, [3] Metallurgy and Ceramics Program, Ames Laboratory, Ames, IA 50011, [4] GDR CINQ, Centre d' Ingénierie des Matériaux, EMN, Parc de Saurupt, F-54042 Nancy

ABSTRACT

We have investigated formation of oxides on quasicrystalline and crystalline alloy surfaces of similar composition, in different oxidizing environments. This includes a comparison between a quaternary orthorhombic approximate of Al-Cu-Fe-Cr quasicrystal and the ternary Al-Cu-Fe quasicrystalline and crystalline phases. We noted that each sample showed the following common trends: preferential oxidation of the Al, enrichment in the concentration of Al present at the surface upon oxidation, water concentration is directly related to oxide thickness, and the oxide thickness displays a strong correlation with the bulk concentration of Al in the sample.

INTRODUCTION

Oxidation is one of the most fundamental of chemical reactions because it is omnipresent in nature, and its inhibition is a crucial property for determining the viability of useful materials. Quasicrystals are thought to manifest low chemical reactivity [1] due to the presence of a pseudogap [2]. Previously, we have investigated the oxidation of the icosahedral phase of Al-Pd-Mn, and have reported preliminary results for Al-Cu-Fe [3]. Other workers have examined the temperature- and pressure-dependence of oxidation on Al-Cu-Fe quasicrystals [4]. Our goal is to (1) identify the components which oxidize, (2) measure the thickness of the oxide, (3) quantify variation in the surface composition, and (4) examine the uniqueness of quasicrystals versus crystals of similar compositions.

EXPERIMENT

Details of sample preparation are given elsewhere [3]. Most germane to the present work is the preparation of the two quasiscrystalline phases. The first is an icosahedral, ternary alloy (ψ-phase). This sample has bulk composition $Al_{65.7}Cu_{22.2}Fe_{12.1}$, based upon inductively-coupled plasma atomic emission spectroscopy (ICP-AES). It is prepared in Ames from a gas-atomized powder, 10-45 μm, which is transformed into a dense solid by hot-isostatic-pressing (HIPing) at 1075 K. The second is an orthorhombic approximate to the quasicrystalline decagonal phase (d-phase), with a roughly estimated bulk composition of $Al_{70}Cu_9Fe_{10.5}Cr_{10.5}$. It is prepared in Nancy by sintering 25-63 μm powders at 1.02 MPa to a final temperature of 1183K. Comparisons are also made to the ternary β- and λ-phases, with compositions of $Al_{51.1}Cu_{34.6}Fe_{14.3}$, and $Al_{74.6}Cu_{3.0}Fe_{22.4}$, respectively.[3]

All samples were polished down to 0 .25 μm diamond paste. They were then examined with scanning electron and Auger microscopies, and X-ray diffraction, to document initial surface composition, porosity, phase purity, and any other notable characteristics. Samples were inspected with these same probes periodically during the study, and after completion of the study to document any changes.

Mat. Res. Soc. Symp. Proc. Vol. 553 © 1999 Materials Research Society

For the XPS study each sample was cleaned in the UHV chamber with a combination of Ar^+ ion sputtering and high temperature annealing. The annealing treatment was developed such that the surface composition was: (1) free of oxides and impurities, (2) reasonably close to the bulk composition (within 3-4 atomic %), and (3) reproducibly stable. The final annealing temperature for both the ψ- and d-phases was 850K.

Three passivating oxidizing environments were used: (1) vacuum oxidation with 99.99% pure oxygen, (2) normal air oxidation within a He-purged sample box containing a $CaSO_4$ desiccant (humidity << 1%), and (3) immersion in Micropore™ purified H_2O. Before oxidizing in any of the environments the sample is cleaned and annealed using the aforementioned technique.

Other details of these procedures are the same as published previously [3].

RESULTS

Figure 1 demonstrates the effect of the standard oxidizing environments upon the pure metal components of Al, Cu, and Fe. In this figure two separate Cu lines are shown in the first and fourth columns to show the formation of the two distinct copper oxides. The first column shows the Cu $2p_{3/2}$ line where one would observe the formation of CuO or the copper hydroxide, $Cu(OH)_2$. The X-ray induced Auger electron spectroscopy (XAES) line of copper, in the last column, is needed to show formation of the reduced Cu (I) oxide, Cu_2O. Close inspection of this figure shows no oxidation in the Cu $2p_{3/2}$ line in any of the oxidizing environments, but Cu_2O is observed to form in both normal air (3^{rd} row) and in water (4^{th} row). The effect of the oxidizing environments on a pure Cu (111) single crystal is formation of Cu_2O in normal air and in water. The second column in the figure shows the effect of the oxidizing environments upon a pure iron single crystal, Fe (110). When the clean crystal is oxidized in vacuum (2^{nd} row), a small amount of iron oxide is observed. By removing the clean sample into normal air, a much thicker iron oxide is promoted. Water has a similar effect. Oxidation of an Al (111) single crystal is displayed in the third column. In vacuum, a thin aluminum oxide is observed. This oxide increases in thickness as one proceeds from vacuum oxidation to normal air oxidation to water immersion. These spectra displayed in Figure 1 provide a baseline for discussing the oxidation of alloys in the Al-Cu-Fe and Al-Cu-Fe-Cr systems.

Figure 2 shows oxidation of the ψ-phase Al-Cu-Fe sample. One additional column is displayed to show the increasing presence of oxygen on the sample surface. Some aspects of this figure are worth noting. The first is that Al is the only component to oxidize *in-situ*. Oxidizing in the other environments promotes formation of a thicker oxide layer while attenuating the signal arising from the Fe and Cu components. The result of this is an Al-rich oxide, with the surface enrichment in Al being proportional to the degree of oxidation. The results for the two crystalline alloys, λ- and β-phase, are very similar. In the Cr-containing alloy, the Cr undergoes some oxidation under all conditions.

Table 1 displays the measured oxide thickness for the two quasicrystalline phases. A comparison is provided between thicknesses measured via fixed angle. Compositional variations in the two quasicrystalline phases are also shown. It can be seen that oxidation induces similar compositional changes, as well as similar oxide thicknesses, for both alloys.

Figure 3 is a collage of variable angle photoelectron spectra for both the Al-Cu-Fe and Al-Cu-Fe-Cr samples. The oxidizing conditions are the same for each sample. The first row of panels display variable angle spectra obtained after the samples were oxidized in vacuum to the point of passivation. There is an additional plot in this set of panels that examines the dependence of the natural log of the ratio of the aluminum oxide signal to the aluminum metal signal versus the inverse sine of the emission angle.

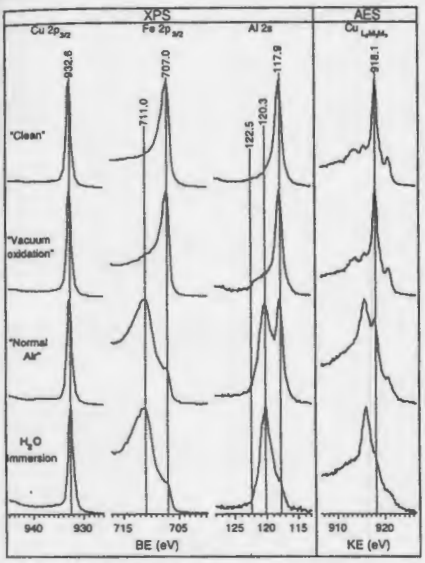

Figure 1. XPS for oxidation of pure metal single crystals corresponding to components found in Al-Cu-Fe alloys. Lines indicate positions of peak for clean metal and associated oxide. Reprinted with permission from Taylor & Francis Ltd, from Ref. 3.

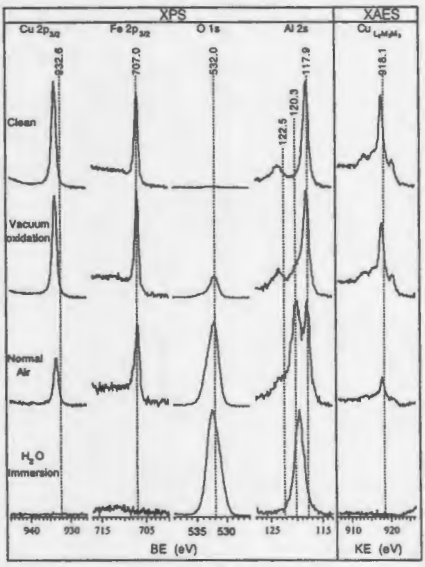

Figure 2. XPS for oxidation of ψ-phase Al-Cu-Fe sample taken at a fixed emission angle of 45° with monochromatic $Al_{K\alpha}$ X-rays. Lines are the same as those for clean metals and associated oxides.defined in Figure 1. Reprinted with permission from Taylor & Francis Ltd, from Ref. 3.

Phase & Environment	n	% Al	% Cu	% Fe	% Cr	Fixed Angle XPS Oxide (Å)	Variable Angle XPS Oxide (Å)
<u>ψ–phase Al-Cu-Fe:</u>							
bulk (ICP-AES)	1	65.7	22.2	12.1			
surface / clean	8	65 ± 1.8	26 ± 3.0	9.2 ± 2.0			
surface / vacuum O_2	3	70 ± 3.0	22 ± 2.3	7.7 ± 1.1		4.7 ± 1.0	5.5 ± 0.5
surface / normal air	3	88 ± 1.1	7.3 ± 1.1	5.0 ± 0		21 ± 0.5	19 ± 1.1
surface / H_2O liquid	2	99 ± 1.4	0 ± 0	1.0 ± 1.4		86 ± 4.3	86 ± 9.6
<u>approx. Al-Cu-Fe-Cr:</u>							
bulk (ICP-AES)	1	70.0	9.0	10.5	10.5		
surface / clean	6	71 ± 2.3	8.2 ± 2.3	12 ± 2.1	8.6 ± 1.0		
surface / vacuum O_2	2	74 ± 1.4	6.5 ± 1.4	11 ± 1.4	9.0 ± 0	4.9 ± 1.1	5.2 ± 0.3
surface / normal air	2	86 ± 2.8	2.0 ± 2.8	7.0 ± 0	5.0 ± 1.4	27 ± 1.4	26 ± 4.2
surface / H_2O liquid	2	95 ± 2.8	0.5 ± 1.4	3.5 ± 1.4	3.5 ± 1.4	70 ± 3.6	75 ± 9.7

Table 1. Compositions of ψ-phase Al-Cu-Fe and the orthorhombic quasicrystalline approximate Al-Cu-Fe-Cr, after various treatments. The two rightmost columns display oxide thickness measured with a fixed take-off angle (45°) and with a variable angle.[3]

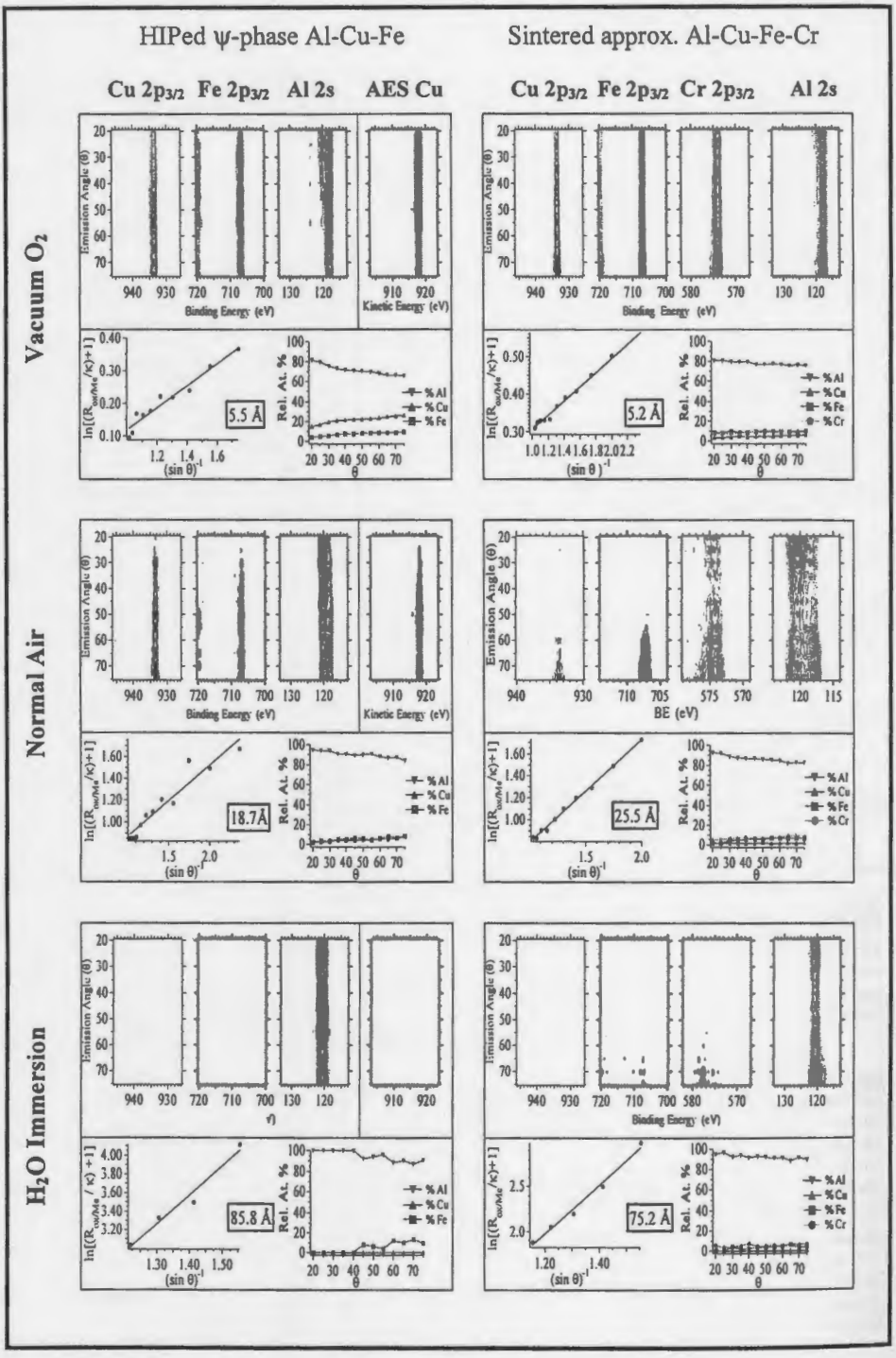
HIPed ψ-phase Al-Cu-Fe
Sintered approx. Al-Cu-Fe-Cr
Cu 2p3/2 Fe 2p3/2 Al 2s AES Cu
Cu 2p3/2 Fe 2p3/2 Cr 2p3/2 Al 2s
Vacuum O2
Normal Air
H2O Immersion
Emission Angle (θ)
Binding Energy (eV)
Kinetic Energy (eV)
BE (eV)
5.5 Å
5.2 Å
18.7Å
25.5 Å
85.8 Å
75.2 Å
Rel. At. %
% Al
% Cu
% Fe
% Cr
(sin θ)-1
θ

Figure 3 (preceding page). Variable angle XPS for HIPed ψ-phase Al-Cu-Fe (left column of panels) and the sintered quasicrystalline approximate Al-Cu-Fe-Cr sample (right hand column of panels). The top row of panels display spectra obtained after vacuum oxidation in the UHV chamber. The pair of panels in the second row show the effect of normal air upon each surface, and the final pair are after H_2O immersion.

The slope of this plot is an accurate measure of the thickness of the oxide layer. This measurement yields a thickness of 5.5Å for Al-Cu-Fe and 5.2Å for the Al-Cu-Fe-Cr. An enrichment of Al in the more surface sensitive region is observed in both samples. As each sample is exposed to a higher degree of oxidation, a thicker passive oxide layer is measured: 18.7Å for Al-Cu-Fe and 25.5Å for Al-Cu-Fe-Cr in normal air. In addition, the surface of each sample becomes more Al rich. This third row of panels displays an additional piece of information which seems a bit peculiar: the aluminum oxide feature for the normal air oxidation of Al-Cu-Fe-Cr shows two distinct maxima: one at the outer surface and another at 65-70° (~80Å below the surface). When these samples are oxidized in water, aluminum oxide is the primary species observed. The Al-Cu-Fe-Cr sample shows chromium oxide at high emission angles. This is particularly obvious after liquid immersion. This indicates that it lies deep in the oxide layer, perhaps at the metal-oxide interface. The oxide depths for Al-Cu-Fe and Al-Cu-Fe-Cr are 85.8Å and 75.2Å, respectively.

Figure 4 shows the aluminum oxide thickness versus a function aluminum content (100% - %Al) in the sample, after vacuum oxidation at room temperature. There appears to be a good linear correlation between these two quantities.

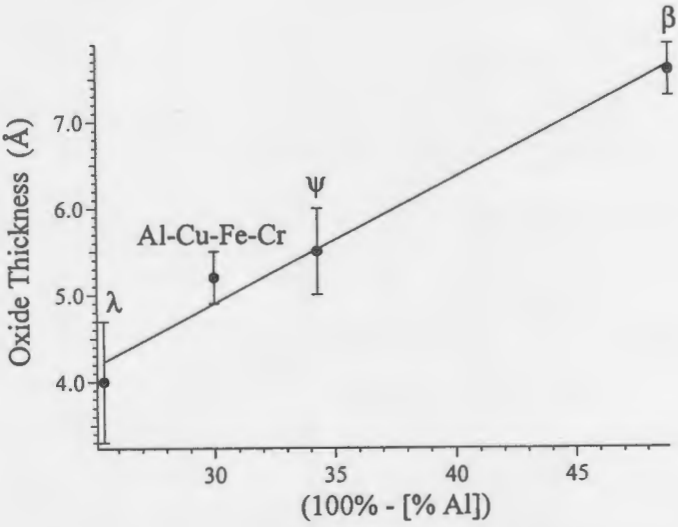

Figure 4. Correlation between the oxide thickness following vacuum oxidation, and the concentration of aluminum in the sample. The line shows a least-squares fit.

CONCLUSION

We observe four noteworthy phenomena. First, in each oxidizing environment, the Al in each alloy is oxidized. This aluminum oxide protects the Cu and Fe (but not the Cr) components from oxidizing, even in environments where they would oxidize as pure metals. Second, the surface becomes enriched in Al as a result of oxidation, with a corresponding depletion in Cu and Fe. The relative compositional change follows a similar trend for each of the alloy systems: Al-Cu-Fe (ψ-phase, β-phase, and λ-phase) and the orthorhombic approximate of the Al-Cu-Fe-Cr d-phase. Third, the oxide depth increases with the severity of the oxidizing environment: 4-8 Å for vacuum oxidation, 19-26 Å for normal air oxidation, and 58-86 Å for water immersion. This points to the importance of humidity and water, and possibly also pressure [4] in the oxidation of these alloys in real environments. Finally, the thickness of the oxide formed via vacuum oxidation varies linearly with the concentration of Al in the sample, suggesting that it is the bulk Al concentration which controls the surface reactivity toward oxidation, at least under these mild conditions.

ACKNOWLEDGEMENTS

This work was supported by the Director, Office of Energy Research, Office of Basic Energy Sciences, Materials Sciences Division, of the U.S. Department of Energy under Contract No. W-405-Eng-82 and by CNRS – France.

REFERENCES

1. N. Rivier in *New Horizons in Quasicrystals: Research and Applications*, edited by A. I. Goldman, D. J. Sordelet, P. A. Thiel, and J. M. Dubois (World Scientific, Singapore, 1997) p. 188.

2. E. Belin-Ferré, V. Fournée, and J.M. Dubois in *New Horizons in Quasicrystals: Research and Applications* (Ref. 1) p. 9.

3. S.-L. Chang, J.W. Anderegg and P.A. Thiel, J. Non-cryst. Solids, 195, 95 (1996); also P.J. Pinhero, S.-L. Chang, J.W. Anderegg, and P.A. Thiel, Phil. Mag. B., 75, 271 (1997); also C. J. Jenks, P. J. Pinhero, S.-L. Chang, J.W. Anderegg, M.F. Besser, D.J. Sordelet, and P.A. Thiel in *New Horizons in Quasicrystals: Research and Applications* (Ref. 1) p. 157; also C. J. Jenks, P. J. Pinhero, T. E. Bloomer, S.-L. Chang, J. W. Anderegg, and P. A. Thiel in *.Proceedings of the Sixth International Conference on Quasicrystals (ICQ6),* edited by S Takeuchi and T. Fujiwara (World Scientific, Singapore, 1998); also P.J. Pinhero, J.W. Anderegg, D.J. Sordelet, M.F. Besser and P.A. Thiel, Phil. Mag. B, in press (1998).

4. D. Rouxel, M. Gravatz, P. Pigeat, B. Weber, and P. Plaindoux in *New Horizons in Quasicrystals: Research and Applications* (Ref. 1) p. 173; also M. Gavatz, D. Rouxel, D. Claudel, P. Pigeat, B. Weber, and J. M. Dubois in *Proceedings of the Sixth International Conference on Quasicrystals (ICQ6),* edited by S Takeuchi and T. Fujiwara (World Scientific, Singapore, 1998).